High-pressure crystalline polyethylene studied by x-ray diffraction and *ab initio* simulations

L. Fontana,[1] Diep Q. Vinh,[2] M. Santoro,[1,4,*] S. Scandolo,[3] F. A. Gorelli,[1,4] R. Bini,[1,5] and M. Hanfland[6]
[1]*LENS, European Laboratory for Non-linear Spectroscopy and INFM, Via N. Carrara 1, I-50019 Sesto Fiorentino, Firenze, Italy*
[2]*International School for Advanced Studies (SISSA), Via Beirut 2-4, 34014 Trieste, Italy*
[3]*The Abdus Salam International Centre for Theoretical Physics (ICTP) and INFM/Democritos National Simulation Center, 34014 Trieste, Italy*
[4]*CRS-SOFT-INFM-CNR, c/o Università di Roma "La Sapienza," I-00185 Roma, Italy*
[5]*Dipartimento di Chimica dell'Università di Firenze, Via della Lastruccia 3, I-50019 Sesto Fiorentino, Firenze, Italy*
[6]*European Synchrotron Radiation Facility, BP 220, F38043 Grenoble, France*
(Received 13 December 2006; revised manuscript received 24 February 2007; published 23 May 2007)

Crystalline polyethylene was investigated under pressure between 0 and 40 GPa, up to 280 °C, by means of synchrotron x-ray powder diffraction and *ab initio* calculations. A rich polymorphism was unveiled, consisting of two new high-pressure monoclinic phases, in addition to the well-known orthorhombic one, which appear reversibly, although with strong hysteresis, upon increasing pressure above 6 GPa ($P2_1/m$, $Z_{chain}=1$) and 14–16 GPa ($A2/m$, $Z_{chain}=2$), respectively. The equation of state was determined for the three solid phases. We find that polyethylene is characterized by a sharp separation between strong covalent intrachain and weaker interchain interactions up to the maximum investigated pressure, which, in turn, places the ultimate chemical stability limit of polyethylene far beyond these thermodynamic conditions.

DOI: 10.1103/PhysRevB.75.174112 PACS number(s): 61.50.Ks, 62.50.+p, 61.10.Nz, 31.15.Ar

I. INTRODUCTION

Polyethylene is the most widely used polymeric material and an important model system in fundamental polymer science, but investigations of its structural behavior under extreme pressure and temperature conditions have so far been very limited. Polyethylene is an archetypal system among one-dimensional polymers and, in the ordered crystalline state, its dynamical properties can be regarded as a textbook example of a one-dimensional harmonic chain.[1] Binding in polyethylene is controlled by a wide range of microscopic interactions, from the strong intrachain covalent C-C and C-H bonds to the weak interchain van der Waals interactions. As a consequence, polyethylene is very stiff if compressed along the chain axis and very soft if compressed along directions perpendicular to the chain axis. The balance between the different microscopic interactions can be strongly altered by the application of pressure and results in a sequence of phase transitions which may ultimately lead to chemical dissociation. Polymorphism in solid polyethylene has been extensively investigated in the past few decades, but only in the moderate pressure regime, e.g., at $P<2-3$ GPa (phase diagram in Fig. 1).[2,3] Polyethylene is generally obtained as a mixture of crystalline and amorphous components. The crystalline material at room conditions is known to exhibit an orthorhombic structure (*Pnam* space group), with two polymeric chains per unit cell. In this phase, the two planes containing the skeletal C chains are almost orthogonal to each other[4] (simulated structure in Fig. 2). In a high-pressure x-ray-diffraction study extended up to 0.3 GPa, the linear compressibility along the chain axis direction was found to be 1 order of magnitude lower than along the orthogonal directions.[5] The equation of state (EOS) of solid polyethylene was also investigated in the *P-T* range of 0–2.5 GPa and 295–373 K by means of isothermal compressibility measurements.[6,7] A second high-pressure–high-temperature crystalline phase, with a stability field located above 200 °C and 0.3 GPa, intermediate between the orthorhombic phase and the liquid state, has been characterized by differential thermal analysis, x-ray-diffraction, and optical microscopy methods.[2,8–12] This phase is hexagonal and partially disordered, as polymeric chains lose the ordered, *all-trans* conformation of the orthorhombic phase. The presence of the hexagonal phase in the phase diagram of polyethylene is crucial for the growth of high-quality crystals of the orthorhombic

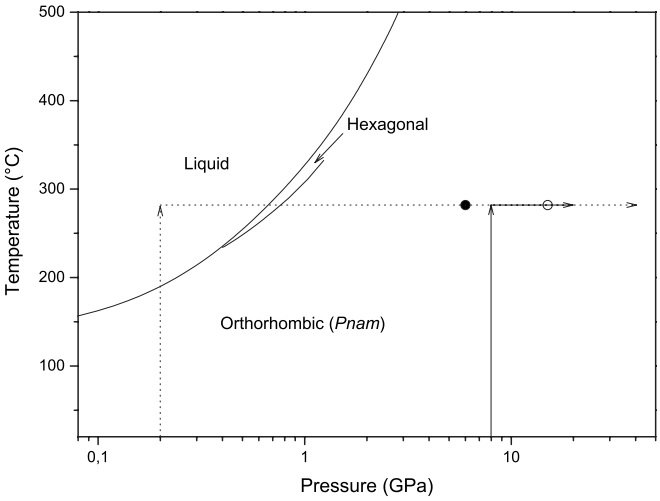

FIG. 1. Phase diagram of liquid and crystalline polyethylene. The present knowledge was limited at $P<2-3$ GPa and $T<500$ °C (see text for extensive references). Specifically, two solid phases were identified within that pressure range: orthorhombic (*Pnam*) and hexagonal polyethylene. Arrows schematically track typical *P-T* paths followed in our study. Dotted line arrows: without pressure medium; full line arrows: argon as a pressure medium. Full and open dots indicate the pressure points where the new $P2_1/m$ and $A2/m$ monoclinic phases started to be observed, respectively, upon increasing pressure.

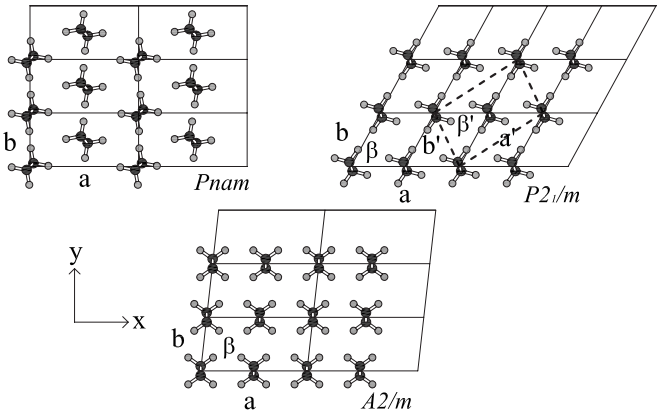

FIG. 2. *Ab initio* simulated unit cells of crystalline polyethylene at ambient pressure in the orthorhombic *Pnam*, monoclinic $P2_1/m$, and $A2/m$ structures, respectively. Polymer chain axes are orthogonal to the drawings. An orthorhombiclike unit cell is also drawn for the $P2_1/m$ structure (dashed lines) to emphasize the similarity to the *Pnam* structure.

phase. In fact, it was shown that chain extended growth always arises when polyethylene is crystallized from the melt through the hexagonal phase, whereas chain-folded growth occurs when the melt is crystallized directly into the orthorhombic phase.[8,12] A third crystal modification of polyethylene is known to occur when the polymer is subjected to stress, e.g., to uniaxial compression.[13] This form has been identified as a monoclinic phase with space group $C2/m$,[13] or equivalently $A2/m$. It has been recognized to be metastable under ambient conditions, as it tends to back transform to the orthorhombic phase upon temperature annealing at ambient pressure.[14] The unit cell of the monoclinic phase contains two chains, with skeletal planes parallel to each other (simulated structure in Fig. 2), but with chains shifted with respect to one another by half of the chain periodicity, along the monoclinic axis. Equivalently, the two chains can be seen as mutually rotated by 180° along the same axis. Pressure evolution of the lattice parameters of monoclinic polyethylene was investigated by x-ray diffraction up to 1.8 GPa,[15] and the compression resulted to be highly anisotropic, similar to the orthorhombic phase.

Only a few theoretical studies have focused on the EOS of crystalline polyethylenes. A model for arbitrary mixtures of amorphous and orthorhombic polyethylenes was developed by Pastine[16] based on the calculation of the lattice potential energy and of the vibrational free energy with empirical interatomic potentials. The model compared favorably with experimental data up to about 1.5 GPa. A similar model was developed by Kobayashi, who also included the contribution of the zero point energy.[17] In this study, the EOSs of orthorhombic and $A2/m$ polyethylene were calculated up to about 1 GPa and it was shown that the orthorhombic structure is always more stable than the $A2/m$, at least at temperatures higher than 130 K. More recently, density-functional calculations were performed on orthorhombic polyethylene up to 10 GPa.[18] The calculations gave structural parameters in fair agreement with diffraction data and confirmed the high anisotropy of this material.

In this paper, we present the results of a combined experimental and theoretical work which extends the investigated pressure range of crystalline polyethylene up to 40 GPa, more than 1 order of magnitude larger than previous experimental investigations. A combination of x-ray-diffraction analysis and *ab initio* calculations is used to show that orthorhombic polyethylene transforms reversibly to a new monoclinic phase above 6 GPa. A further phase transition occurs above 14–16 GPa to another monoclinic phase which was identified as isostructural to the metastable form reported in stressed polymers at ambient conditions.

II. EXPERIMENTAL PROCEDURES

Crystalline polyethylene samples from Aldrich (UHMW, $M_w=3\times10^6-6\times10^6$, density=0.94 g/cm^3) were loaded in LeToullec-type membrane diamond-anvil cells (MDACs) equipped with 400 μm culet diamond anvils and rhenium or Inconel gasket. The sample chamber diameter and initial thickness were equal to about 150 and 40 μm, respectively. The pressure was measured from the shift of the $^5D_0$-$^7F_0$ luminescence line of $SrB_4O_7:Sm^{2+}$ [5 mol % of divalent samarium in SrB_4O_7 (Ref. 19)] using the calibration given by Datchi *et al.*[20] A chip of this optical sensor (size of the grain $\sim$1 μm) was inserted in the sample chamber. Temperatures up to 300 °C were obtained by resistive heating of the cell. The temperature was measured by a J-type thermocouple, which was placed close to the copper ring clamping the diamond anvil. The uncertainty of the temperature measurements was estimated to be 3 °C.

Different samples were loaded in the MDAC with argon as a pressure medium (high-pressure loading) and without pressure medium. The as-loaded samples always exhibited, at pressures of 0.1–3 GPa, a finite amount of metastable monoclinic phase and of amorphous material, together with the dominant orthorhombic component. Specifically, the presence of the monoclinic phase is mostly a consequence of the amount of stress that was produced in the samples by the loading procedures. Thermal annealing of samples was then mandatory for removing the monoclinic and the amorphous spurious phases before facing the structural investigation of crystalline polyethylene in the most ideal conditions. In the case of samples loaded without pressure medium, a proper thermal annealing procedure turned out to consist in recrystallizing polyethylene from the melt, through the hexagonal phase, upon pressure increase from 0.2 GPa at 280 °C (chain extended growth), as schematically indicated in Fig. 1. Indeed, in this way, we obtained a high-quality orthorhombic phase, showing quite narrow [full width at half maximum (FWHM) of (110) and (200) lines=0.07° and 0.09° at 2.5 GPa, respectively] and homogeneous Debye-Sherrer rings [see Fig. 3(a) and, in the following, Fig. 5(a)], apart from a slight amount of amorphous component. In Fig. 4(a), a low angle section of the diffraction pattern measured in this kind of samples at 7.6 GPa and 280 °C is reported. Here, we observe the two strongest (110) and (200) peaks of the *Pnam* phase, still reasonably sharp (FWHM=0.09° and 0.12°, respectively), along with a weak peak positioned at about 6.98°, in between the two orthorhombic lines, which indicates that a phase transition is occurring to a new phase, as extensively discussed in the following. In addition, a very

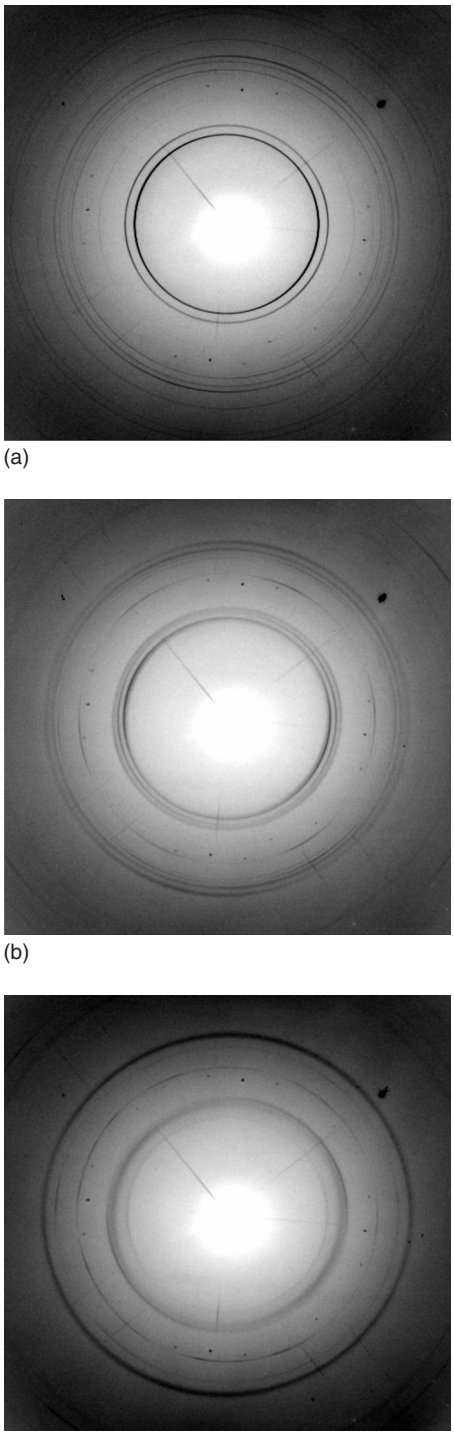

FIG. 3. Sections of the diffraction images showing the Debye-Sherrer rings at three different pressures, (a) 2.7 GPa, (b) 15.5 GPa, and (c) 40.4 GPa, corresponding to the patterns reported in Fig. 5.

weak and broad band is evident at the low angle side of the (110) *Pnam* peak, marking the presence of remnants of the amorphous material. When argon was employed as a pressure medium, the possibility to recrystallize polyethylene from the melt at high temperatures, at a few tenths of gigapascals, was prevented because of the difficulty in controlling the sealing of argon at those *P-T* conditions. In this case,

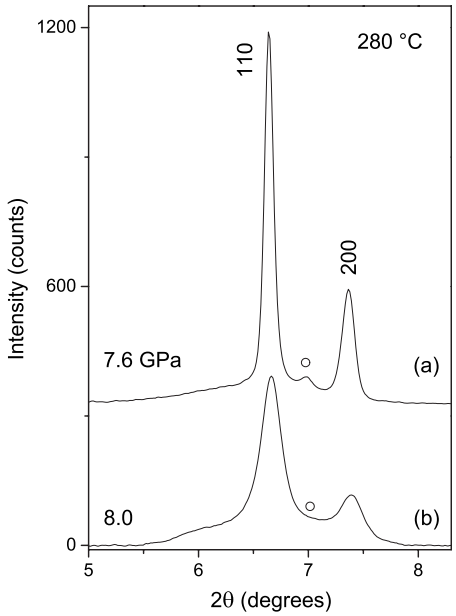

FIG. 4. Detail of x-ray-diffraction patterns measured around 8 GPa on a polyethylene sample loaded (a) without pressure medium and (b) with argon as the pressure medium and thermally annealed as described in the text. The two strongest peaks, labeled by Miller indices, belong to the orthorhombic *Pnam* phase, while open dots mark an extra peak that points to a new high-pressure phase.

the thermal annealing procedure was limited to heat the solid polymer in the range of a few gigapascals up to 200–300 °C, as schematically reported in Fig. 1. In Fig. 4(b), we report a limited section of a diffraction pattern of this kind of samples, measured at 8.0 GPa and 280 °C. The (110) and (200) peaks of the orthorhombic phase are much broader (FWHM=0.24° and 0.21°, respectively) than in the sample loaded without pressure medium. Also, the weak peak assigned to the new crystalline phase is hardly detectable as a high angle shoulder of the (110) *Pnam* line, at about 7.0°, while the remarkable intensity at the low angle side of the (110) peak points to a more relevant amount of residual monoclinic and, eventually, amorphous phases. Pressure behavior of this kind of samples was qualitatively similar to the one exhibited by samples loaded without pressure medium. On the other hand, since pure polyethylene samples exhibited a much higher crystalline quality and initial phase purity, the determination of structure and phase transformations turned out to be much more precise dealing with these samples. Therefore, we always refer in the following to samples loaded without pressure medium and annealed as described above, unless differently specified. Particularly, we will focus our attention of an isothermal pressure scan performed at 280 °C from 2.5 to 40 GPa. We are aware that the absence of a proper pressure medium limits the precision of our investigation due to nonhydrostatic effects, which are evident in Fig. 6 where we observe pressure induced broadening of the diffraction peaks; nevertheless, our experimental study turned out to be accurate enough for supporting all the main predictions of theoretical simulations.

Angle dispersive x-ray powder diffraction has been measured at the ID09A beamline of the European Synchrotron

Radiation Facility (ESRF, Grenoble). Here, the white beam is vertically focused by a spherical mirror and, horizontally, by a bent silicon (111) monochromator. Finally, we used a monochromatic beam (λ=0.4108 Å) that goes through a cleaning pinhole and forms a circular spot on the sample, whose diameter is equal to 30 μm. The scattered radiation is detected by an image-plate detector (Mar345). The diamond seats, made of tungsten carbide, allowed us to achieve a maximum diffraction angle 2θ of about 24°. The diffraction patterns were analyzed and integrated by means of the FIT2D computer code[21] to obtain the one-dimensional intensity distribution as a function of the 2θ scattering angle.

III. THEORETICAL PROCEDURES

First-principles calculations were carried out within density-functional theory, as implemented in the Quantum ESPRESSO code.[22] The total energy of a given atomic configuration was obtained using the Perdew-Burke-Ernzerhof (PBE)[23] parametrization of the exchange correlation potential. The ion-electron-interaction was described by ultrasoft pseudopotentials,[24] and electronic wave functions were expanded in a plane-wave basis set with kinetic-energy cutoff of up to 110 Ry. Brillouin zones were sampled with up to 52 special points. We built a number of structural guesses by considering different orientations and alignments of the polyethylene chains, in unit cells containing up to four chains (eight CH_2 units). Atomic positions were then relaxed to the closest local minimum with a conjugate-gradient method at T=0 K. By selecting among the resulting structures those with the lowest energy allowed us to identify three likely candidates for the crystal structure of polyethylene. Two of them coincide with the known forms of polyethylene, *Pnam* and $A2/m$. The third one was found to have space group $P2_1/m$ and is shown in Fig. 2. Theoretical x-ray-diffraction patterns were constructed using the relaxed atomic positions and atomic structure factors for carbon and hydrogen taken from the literature.[25,26] Uncertainties in the determination of lattice parameters with first-principles methods are generally believed to be of the order of a few percent, but the weak, van der Waals nature of interchain binding in polyethylene requires us to be more cautious, as the asymptotic $1/r^6$ tail of the van der Waals potential is not accounted for by local approximations to density-functional theory such as the ones used in this work. Nonetheless, the study of Miao *et al.*,[18] which was based on approximations very similar to the ones employed here, shows that the lattice parameters of the orthorhombic phase agree with experimental data within 1%–3%. Moreover, the reduction of the interchain distance induced by the application of pressure reduces the van der Waals problem considerably at high pressures. Our theoretical values for the lattice parameters of crystalline polyethylene are listed in Table I and show an excellent agreement with experimental data, as shown in the following section.

The interpretation of the experimental patterns at high pressure was based on the assumption that the complexity of the patterns is a consequence of the coexistence of more than one phase, among the three phases shown in Fig. 2. The theoretical lattice parameters calculated for each phase were employed as a starting guess to fit the experimental patterns. The success of this procedure in reproducing the observed patterns, which we discuss in detail in the next section, leads us to the conclusion that the three phases shown in Fig. 2 provide a complete description of the behavior of polyethylene under compression and that no additional phases are required to describe its phase diagram in the pressure range studied. Measured intensities and measured and/or fitted peak positions differ with respect to theoretical ones, always within the range of accuracy expected for our *ab initio* approach.

IV. RESULTS AND DISCUSSION

Experimental and theoretical diffraction patterns of crystalline polyethylene are reported in Fig. 5 (intensities and peak positions in Table I) at three selected pressures. Although we achieved a maximum diffraction angle 2θ of about 24°, in Fig. 5, we limited the range to 14° for not compressing the most relevant features [see a typical pattern up to 24° in the inset of Fig. 5(a)]. On the other hand, above 14°, we only observed weak peaks of the orthorhombic phase, whose structure is very well assessed. A complete information on peaks observed above 14° is provided in Table I. At 2.6 GPa, the crystalline sample is in a pure orthorhombic *Pnam* phase, exhibiting up to 25 diffraction peaks [Fig. 5(a) and Table I]. A shallow remnant of amorphous component is inferred from the presence of a broad band centered at about 2θ=5.8°. Above 6 GPa, a new phase appears, as indicated by the appearance of a new peak between the strong 110 and 200 lines of the orthorhombic phase (see Figs. 4 and 6 at 7.6 GPa). The peak intensities of the new phase increase slowly with pressure, while peaks of the orthorhombic phase weaken. This is in agreement with our theoretical results, shown in Fig. 7, which indicate that a new monoclinic phase ($P2_1/m$, see Fig. 2) becomes more stable than the *Pnam* structure above 4±1 GPa. The error on the transition pressure reflects the error of the calculated energies (±5 meV). The monoclinic phase contains one chain only per unit cell, and its structure can be related to that of the orthorhombic phase by considering an orthorhombiclike cell obtained by doubling the $P2_1/m$ unit cell as shown by the dashed lines in Fig. 2. The dashed orthorhombiclike cell of the $P2_1/m$ phase differs from that of the *Pnam* phase by a small departure from 90° (the value in the orthorhombic phase) of the angle β' between the two axes perpendicular to the chain direction (a′ and b′ in Fig. 2) and by the setting angle (i.e., the angle between the polymeric planes and the a axis of the orthorhombic phase), which is almost 90° for the monoclinic phase and has a value ranging from 45° to 90° for the orthorhombic phase.[18]

The experimental pattern at 15.5 GPa in Fig. 5(b) can be essentially indexed as a mixture of the *Pnam* (six peaks) and the $P2_1/m$ (five peaks) phases. This is consistent with the theoretical results, which indicate that the two phases are nearly degenerate in energy. In fact, the calculated energy differences between *Pnam* and $P2_1/m$ are, in this pressure range, close to the expected accuracy of our theoretical approach (Fig. 7).

TABLE I. Assignment of the observed and simulated diffraction lines at three different pressures, corresponding to patterns reported in Figs. 3 and 5, according to the *Pnam*, $P2_1/m$, and $A2/m$ crystal structures. The observed and simulated angle positions and integrated intensities are reported, along with the calculated angle positions as obtained by fitting the different structures to the experimental patterns. Lines with double assignment are labeled by asterisks. The comparison between observed and simulated intensities is rather qualitative, most likely due to the limited accuracy of the simulation procedure.

			Pnam			
hkl	2θ (deg) (Simul.) (2.6 GPa)	Intensity (Simul.) (2.6 GPa)	2θ (deg) (Obs.) (2.6 GPa)	Intensity (Obs.) (2.6 GPa)	2θ (deg) (Calc.) (2.6 GPa)	$\Delta 2\theta$ (deg) (Obs.−Calc.)
110	6.060	99	6.231	100	6.233	−0.002
200	6.871	100	6.870	37	6.869	0.001
210	8.497	3	8.616	3	8.620	−0.004
020	9.993	21	10.419	3	10.413	0.006
011			10.649	8	10.654	−0.005
120	10.570	5	10.971	0,3	10.967	0.004
111	11.065	19	11.193	8	11.196	−0.003
310	11.465	20	11.560*	12*	11.555	0.005*
201			11.560*	12*	11.564	−0.004*
220	12.138	9	12.483	1	12.485	−0.002
211	12.572	9	12.682	4	12.687	−0.005
400	13.727	23	13.773	1	13.763	0.010
121	14.040	1	14.389	5	14.392	−0.003
320	14.341	7	14.678	2	14.675	0.003
410					14.722	
311	14.724	5	14.844	4	14.848	−0.004
221	15.254	12	15.575	1	15.585	−0.010
130	15.366	2	16.028	0,3	16.023	0.005
401	16.576		16.634	2	16.631	0.003
230					17.105	
420					17.289	
321	17.090	4	17.406	1	17.396	0.010
411					17.437	
510					18.007	
031	17.628		18.230	1	18.227	0.003
131					18.553	
002	18.555	30	18.637	3	18.645	−0.008
330					18.774	
231	18.932	0,10	19.495	1	19.499	−0.004
421			19.667*	3*	19.661	0.006*
112	19.531	17	19.667*	3*	19.677	−0.010*
202	19.800	18	19.886	1	19.891	−0.005
520					20.171	
511	20.182	2	20.287	1	20.298	−0.011
212					20.573	
600					20.708	
430					20.895	
040					20.913	
331					20.985	
140					21.199	
302	21.259		21.381	1	21.351	0.030

TABLE I. (*Continued.*)

	Cell parameters (Simul.)		Cell parameters (Expt.)			
	a=6.853 Å		a=6.857 Å			
	b=4.716 Å		b=4.527 Å			
	c=2.548 Å		c=2.536 Å			
			Pnam			
hkl	2θ (deg) (Simul.) (15.5 GPa)	Intensity (Simul.) (15.5 GPa)	2θ (deg) (Obs.) (15.5 GPa)	Intensity (Obs.) (15.5 GPa)	2θ (deg) (Calc.) (15.5 GPa)	$\Delta 2\theta$ (deg) (Obs.−Calc.)
110	7.121	61	6.968	100	6.989	−0.021
200	7.604	100	7.683	35	7.700	−0.017
210	9.671	0.2	9.684	3	9.665	0.019
011			11.083	9	11.095	−0.012
020					11.680	
111	11.759	33	11.745	16	11.747	−0.002
201			12.164	3	12.186	−0.022
120	12.578	0,3			12.302	
310	12.883	31			12.958	
211	13.509	0.6	13.512	4	13.519	−0.007
220					14.005	
400	15.029	25	15.411	2	15.436	−0.025
121					15.522	
311	15.921	8	16.073	1	16.050	0.023
320	16.693	1	16.594*	3*	16.463	0.131*
410			16.594*	3*	16.514	0.08*
221	17.233	27	16.911	1	16.910	0.001
130					17.981	
401					18.119	
002					18.924	
321					19.005	
411					19.049	
230					19.197	
420					19.400	
031					19.965	
112					20.196	
510					20.205	
131					20.340	
202	20.300	22	20.465	2	20.458	0.007
330					21.073	
212					21.290	
231					21.427	
421					21.610	
022			22.294	2	22.295	−0.001
511	21.961	7			22.339	
	Cell parameters (Simul.)		Cell parameters (Expt.)			
	a=6.168 Å		a=6.118 Å			
	b=3.992 Å		b=4.037 Å			
	c=2.510 Å		c=2.499 Å			

TABLE I. (*Continued.*)

			P2$_1$/m			
hkl	2θ (deg) (Simul.) (15.5 GPa)	Intensity (Simul.) (15.5 GPa)	2θ (deg) (Obs.) (15.5 GPa)	Intensity (Obs.) (15.5 GPa)	2θ (deg) (Calc.) (15.5 GPa)	$\Delta 2\theta$ (deg) (Obs.−Calc.)
010	6.937	65	6.781	34	6.781	0.000
−110	7.470	100	7.373	100	7.373	0.000
100	7.603	59	7.529	6	7.530	−0.001
011	11.660	20	11.626	22	11.627	−0.001
−111					11.984	
−120	12.297	28			12.014	
101	12.081	19	12.082	65	12.081	0.001
110					12.303	
−210	13.399	24			13.292	
020					13.585	
	Cell parameters (Simul.)		Cell parameters (Expt.)			
	a=7.069 Å		a=7.102 Å			
	b=3.870 Å		b=3.943 Å			
	c=2.513 Å		c=2.498 Å			
	β=118.2°		β=118.2°			
			P2$_1$/m			
hkl	2θ (deg) (Simul.) (40.4 GPa)	Intensity (Simul.) (40.4 GPa)	2θ (deg) (Obs.) (40.4 GPa)	Intensity (Obs.) (40.4 GPa)	2θ (deg) (Calc.) (40.4 GPa)	$\Delta 2\theta$ (deg) (Obs.−Calc.)
010	8.005	56	7.716	100	7.712	0.004
100	7.843	57			7.950	
−110	8.125	100	8.085	24	8.089	−0.004
011	12.445	23	12.229	50	12.233	−0.004
101	12.327	23	12.389	40	12.385	0.004
−111	12.519				12.475	
110					13.434	
−120	14.276	22			13.682	
−210	13.863	23			14.089	
	Cell parameters (Simul.)		Cell parameters (Expt.)			
	a=6.689 Å		a=6.701 Å			
	b=3.429 Å		b=3.454 Å			
	c=2.477 Å		c=2.485 Å			
	β=120.4°		β=117.8°			
			A2/m			
hkl	2θ (deg) (Simul.) (40.4 GPa)	Intensity (Simul.) (40.4 GPa)	2θ (deg) (Obs.) (40.4 GPa)	Intensity (Obs.) (40.4 GPa)	2θ (deg) (Calc.) (40.4 GPa)	$\Delta 2\theta$ (deg) (Obs.−Calc.)
010	6.779	69	6.751	24	6.751	0.000
200	8.147	100	8.085	48	8.085	0.000
101	10.348	0.1			10.281	
−210	10.451	32			10.357	

TABLE I. (*Continued.*)

hkl	2θ (deg) (Simul.) (40.4 GPa)	Intensity (Simul.) (40.4 GPa)	2θ (deg) (Obs.) (40.4 GPa)	Intensity (Obs.) (40.4 GPa)	2θ (deg) (Calc.) (40.4 GPa)	$\Delta 2\theta$ (deg) (Obs.−Calc.)
210	10.815	43			10.720	
−111	12.535	25	12.229	100	12.231	−0.002
111	12.379	22	12.389	81	12.387	0.002
020	13.582	0.5			13.526	
	Cell parameters (Simul.)		Cell parameters (Expt.)			
	a=5.782 Å		a=5.831 Å			
	b=3.440 Å		b=3.491 Å			
	c=2.477 Å		c=2.494 Å			
	β=88.1°		β=92.0°			

At least two strong arguments indicate the *Pnam*-$P2_1/m$ thermodynamic phase transition, observed at 4–6 GPa, to be first order: (i) discontinuity of lattice parameters (see the following) and (ii) extended coexistence of the two structures beyond the transition pressure, which, in turn, points to a strong kinetic barrier between these phases. It is interesting to remark that the pressure evolution of the calculated and experimental lattice parameters and of the calculated internal parameters of the *Pnam* and $P2_1/m$ phases, in the coexistence region above the transition pressure, e.g., in the region where the *Pnam* is metastable with respect to $P2_1/m$, is reminiscent of a quasi-second-order transition between the two phases. Despite the absence of a group-subgroup relationship between the two structures, which would be the required condition in the case of a genuine Landau-type second-order transition, the pressure evolution of the angle β' in the $P2_1/m$ phase is such that it approaches asymptotically the value of 90°, which characterizes the *Pnam* phase. At the same time, the setting angle within the *Pnam* phase tends asymptotically to a value close to 90°, which characterizes instead the $P2_1/m$ phase. The disappearance of the *Pnam* phase with pressure can therefore be seen as a quasi-continuous transformation of the *Pnam* phase into the $P2_1/m$ phase, the latter being the phase that survives at higher pressures.

The weak signature of a third crystalline phase appears in the diffraction patterns starting from 15.5 GPa and consists of an extra peak at about 6.2° (at 15.5 GPa, see Fig. 5(b)). This peak slowly intensifies with pressure. In concomitance with the appearance of this phase, the orthorhombic peaks weaken and vanish at about 30 GPa (Figs. 5 and 6). The theoretical simulations indicate that the monoclinic $A2/m$ phase, which was observed as a metastable phase at ambient conditions,[13] is energetically very close to the $P2_1/m$ phase and also becomes more stable than the *Pnam* structure above 4±1 GPa. Indeed, the enthalpy difference between the $P2_1/m$ and $A2/m$ phases is always less than 5 meV above 4 GPa. Such an energy difference is of the order of the accuracy of our calculations, so we are not in a position to distinguish theoretically the thermodynamically stable phase at high pressure. From the structural point of view, the two phases differ by a relative translation of the chains, as discussed in Sec. I. The new diffraction peak at low angle, seen above 14 GPa, corresponds to the (010) reflection of the $A2/m$ phase. At 40.4 GPa [Fig. 5(c)], the experimental pattern no longer shows remnants of the orthorhombic phase and can be indexed as a mixture of the $P2_1/m$ (four peaks) and the $A2/m$ (four peaks) monoclinic structures. Remarkably, only the (010) peaks are well separated at a given pressure in the two phases, while the other peaks are basically superimposed. This is the consequence of an accidental similarity between the lattice parameters for the two phases. In particular, the lattice parameters of the $P2_1/m$ orthorhombic-like cell indicated by the dashed line in Fig. 2 are basically identical to those of the $A2/m$ cell at all pressures. Therefore, the two structures appear to be very similar in terms of cell shape, in spite of their differences in the internal positions of the chains. On the other hand, the lattice parameters of the orthorhombic *Pnam* phase differ by 5%–7% with respect to those of the $P2_1/m$ and $A2/m$ phases at those pressures where the $P2_1/m$ and $A2/m$ phases start to be experimentally observed, i.e., at about 6 and 14 GPa, respectively. As a consequence of the accidental similarity between the lattice parameters of the $P2_1/m$ and $A2/m$ phases and of the limited number of observed peaks, the structures of these phases were fitted not only to the observed peaks but also to the monoclinic angles as determined by the simulations. After having assigned the peaks of the new monoclinic phase $A2/m$ at 40.4 GPa, we were able to index the patterns in the whole pressure region between 15 and 40 GPa, where we dealt with more complicated situations that involve the coexistence of all the three phases: *Pnam*, $P2_1/m$, and $A2/m$ (Fig. 6). In Fig. 6, selected patterns measured upon pressure release are also reported. The intensity of the $A2/m$ phase component increases upon pressure decrease, with respect to that of the $P2_1/m$ phase component, down to 3.8 GPa, the minimum pressure achieved (see inset of Fig. 6). In another set of experiments, where orthorhombic polyethylene was similarly transformed into the $P2_1/m$ and $A2/m$ phases, the almost pure *Pnam* phase was reversibly recovered at ambient conditions (Fig. 6).

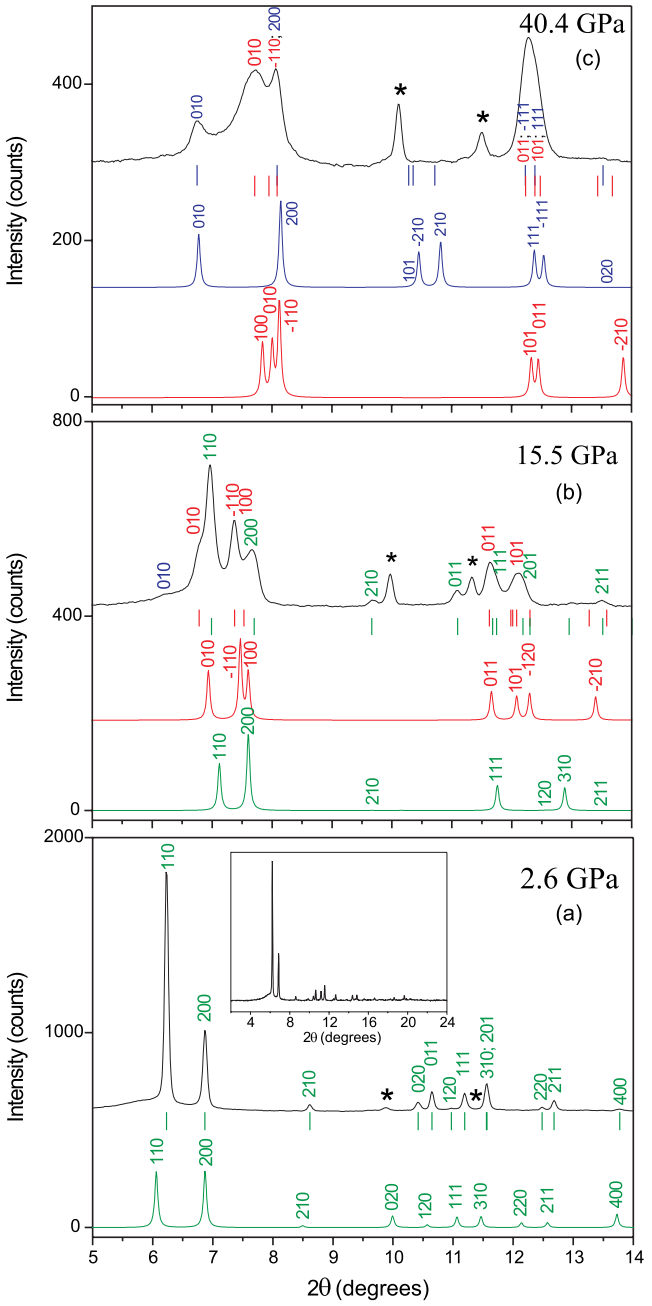

FIG. 5. (Color) Selected x-ray-diffraction patterns (black lines) of crystalline polyethylene at 280 °C, measured upon pressure increase, showing the different phase components occurring at high pressures (see also Fig. 3). The background was subtracted, and then the patterns were vertically shifted. *Ab initio* simulated patterns (theoretical line-widths have been given an arbitrary value of 0.06°) of the orthorhombic *Pnam* (green line), monoclinic $P2_1/m$ (red line), and monoclinic $A2/m$ (blue line) phases are also reported. Vertical sticks: positions of Bragg peaks fitted to the experimental peaks. Miller indices are reported for experimental and theoretical peaks. Colors of vertical sticks and Miller indices correspond to the three phases, as described above. Stars indicate peaks of the rhenium gasket. The reported 2θ region is limited to 14.0°; beyond this angle, no diffraction peaks were observed at pressures in excess of 20 GPa. In the inset of panel (a), we report the diffraction pattern of the orthorhombic phase up to 24°.

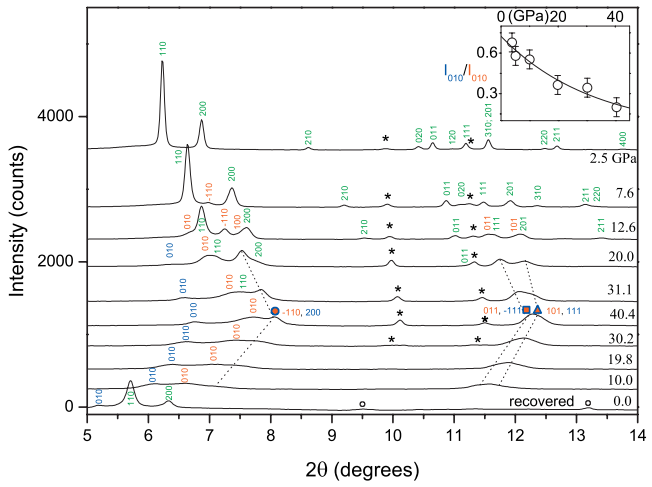

FIG. 6. (Color) Selected x-ray-diffraction patterns measured in a compression-decompression cycle (2.5 to 40.4 to 3.8 GPa) at 280 °C. The background was subtracted. Different colors of Miller indices correspond to the *Pnam* (green), $P2_1/m$ (red), and $A2/m$ (blue) phases, respectively, similar to Fig. 5. Double color dots indicate peaks that correspond to overlapping diffraction lines of the two monoclinic phases, whose pressure shift is traced by dotted lines. The pattern of a typical ambient pressure and temperature recovered sample is also reported after the pressure medium (argon) was let to flow out, showing an almost pure orthorhombic structure, apart from a remnant of $A2/m$ phase. Stars and open dots indicate peaks of the rhenium and Inconel gasket, respectively. Inset: pressure behavior of integrated intensity ratio between the (010) peak of the $A2/m$ and the $P2_1/m$ phases, respectively, measured upon pressure decrease. A guide for the eyes has been drawn through the experimental points.

We interpret the stronger stability of the $A2/m$ phase upon pressure release as an indication that the $P2_1/m$ phase is metastable in the P-T range where it was observed. Therefore, the phase diagram of polyethylene can be likely described, up to 40 GPa, by two phases only, the *Pnam* ortho-

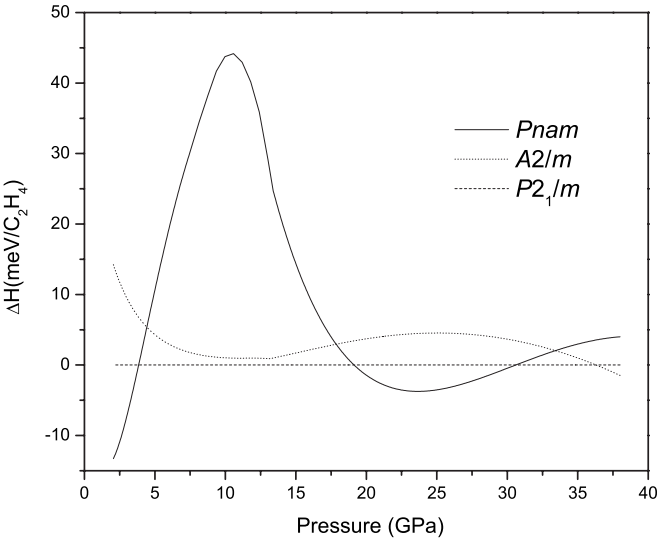

FIG. 7. Enthalpy versus P relative to the $P2_1/m$ phase at $T=0$ K.

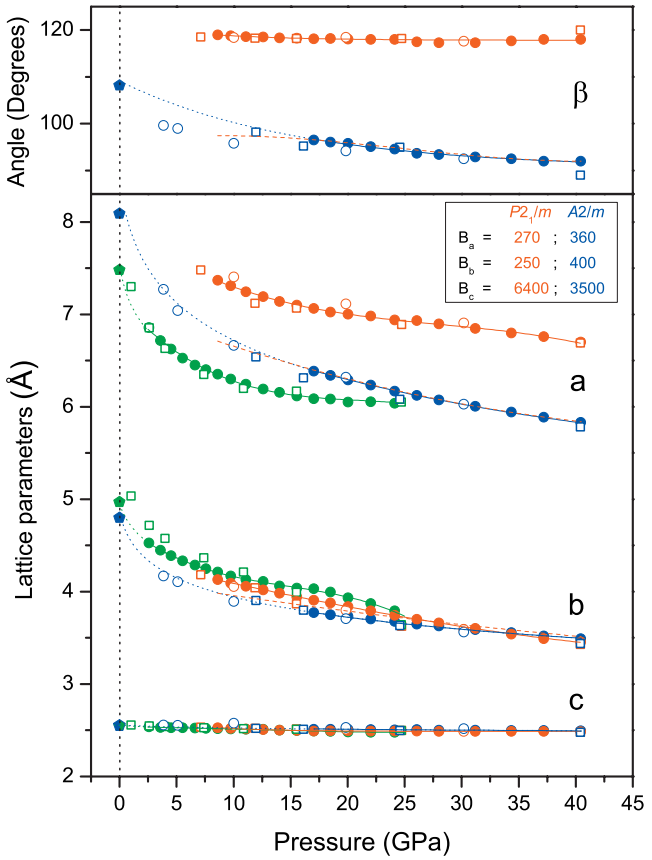

FIG. 8. (Color) Lattice parameters and monoclinic angle β of the *Pnam* (green), $P2_1/m$ (red), and $A2/m$ (blue) phases of polyethylene, respectively: full (open) circles, measured upon pressure increase (decrease); pentagon, experimentally reported at ambient pressure (Ref. 27); and squares, obtained by computer simulations. Phenomenological polynomial curves (continuous lines) have been fitted to the experimental values of the lattice parameters and of the monoclinic angle and have been extrapolated to ambient pressure (dotted lines). Changes from negative to positive values of the curvature are observed (see *a* of $P2_1/m$ and *b* of *Pnam*), most likely related to the strong metastability. The inset table reports the values of the isothermal linear bulk moduli $B_{a_i}=-a_i(\partial a_i/\partial P)^{-1}$, in GPa ($a_1=a$, $a_2=b$, and $a_3=c$), of the $P2_1/m$ and $A2/m$ phases at 40.4 GPa. Dashed lines are polynomial curves fitted to the experimental cell parameters and monoclinic angle of the $P2_1/m$ orthorhombiclike unit cell.

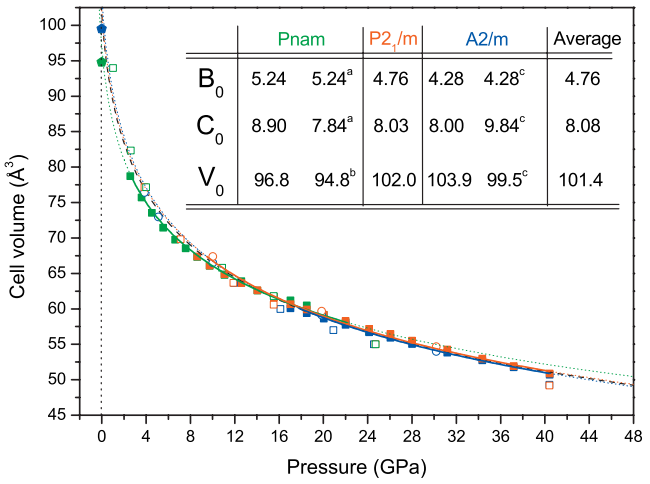

FIG. 9. (Color) Pressure-volume relations of the *Pnam* (green), $P2_1/m$ (red), and $A2/m$ (blue) phases of polyethylene, respectively: full squares (open circles), measured upon pressure increase (decrease); open squares, obtained by computer simulations. Vinet EOSs (Ref. 28) (continuous lines) have been fitted to the experimental values and extrapolated to ambient pressure (dotted lines). In the inset table are reported values of V_0 (in Å^3), B_0 (in GPa), and C_0 for the three phases, separately, and of an average EOS (dashed black line) which has been fitted to the experimental data all together. The B_0 parameter has been constrained to literature values, experimentally reported at lower pressures, for the *Pnam* and the $A2/m$ structures and to the average of those values for the $P2_1/m$ structure. Literature values of B_0, C_0, and V_0 (pentagons in the picture) are reported: (a) Ref. 5, (b) Ref. 27, and (c) Ref. 15.

rhombic phase and the $A2/m$ monoclinic high-pressure phase.

In Figs. 8 and 9, we report the behavior of the structural parameters of all the three phases, *Pnam*, $P2_1/m$, and $A2/m$, over the full investigated pressure range. The comparison between experimental and theoretical results for the lattice parameters and the monoclinic angle β is fairly good. Empirical curves fitted to the experimental data extrapolate reasonably well, for the *Pnam* and $A2/m$ phases, to the experimentally reported ambient pressure values.[27] This confirms that the high-pressure $A2/m$ phase found in this study coincides with the metastable phase observed in stressed samples at ambient conditions.[13] At the maximum pressure of 40.4 GPa, the isothermal linear bulk modulus along the chain direction is still an order of magnitude larger than in orthogonal directions. Such a strong anisotropy indicates that the separation between intrachain covalent and interchain van der Waals interactions persists at high pressures, which is suggestive of a strong chemical stability of polyethylene up to at least 40 GPa, and even above this pressure.

Pressure-volume relations for the three investigated phases have been fitted with a Vinet EOS (Ref. 28) (Fig. 9): $P=3B_0[(1-f)/f^2]\exp[1.5(C_0-1)(1-f)]$, where $f=(V/V_0)^{1/3}$, V_0 is the cell volume at ambient pressure, and B_0 and C_0 are the isothermal bulk modulus and its first pressure derivative at $P=0$, respectively. The present curves are consistent with earlier EOSs determined at lower pressures. We note that data sets corresponding to different phases are very close to each other, so that they can also be reasonably fitted by a single EOS.

V. CONCLUSIONS

The pressure behavior of crystalline polyethylene has been investigated up to 40 GPa on the basis of experimental and theoretical analyses. The compression is characterized by large hysteresis and phase coexistence between the ambient pressure orthorhombic phase and two monoclinic phases. Our analysis suggests that the orthorhombic *Pnam* phase is thermodynamically stable up to about 6 GPa. The *Pnam* phase then transforms into a monoclinic, possibly metastable phase with $P2_1/m$ space group. The high-pressure stable

phase belongs to space group $A2/m$ and appears above 14 GPa.

Polyethylene is found to be chemically stable up to the maximum pressure of this study, equal to 40 GPa. We hope this work will stimulate studies on the physical and chemical properties of other model polymeric materials in a similarly extended range of thermodynamic conditions.

ACKNOWLEDGMENTS

We acknowledge the ESRF for provision of beam time at ID09A. This work has been supported by the European Community, under Contract No. RII3-CT2003-506350, and the by the Ente Cassa di Risparmio di Firenze, through the grant "Firenze Hydrolab."

*Electronic address: santoro@lens.unifi.it

[1] N. W. Ashcroft and N. D. Mermin, *Solid State Physics* (Holt, Rinehart and Winston, New York, 1976).
[2] D. C. Bassett and B. Turner, Nature (London), Phys. Sci. **240**, 146 (1972).
[3] M. Hikosaka, S. Minomura, and T. Seto, Jpn. J. Appl. Phys. **14**, 589 (1975).
[4] C. W. Bunn, Trans. Faraday Soc. **35**, 482 (1939).
[5] T. Ito and H. Marui, Polym. J. (Tokyo, Jpn.) **2**, 768 (1971).
[6] R. W. Warfield, J. Appl. Chem. **17**, 263 (1967).
[7] Y. Zhao, J. Wang, Q. Cui, Z. Liu, M. Yang, and J. Shen, Polymer **31**, 1425 (1990).
[8] D. C. Bassett, S. Block, and G. J. Piermarini, J. Appl. Phys. **45**, 4146 (1974).
[9] M. Yasuniwa, R. Enoshita, and T. Takemura, Jpn. J. Appl. Phys. **15**, 1421 (1976).
[10] T. Yamamoto, H. Miyaji, and K. Asai, Jpn. J. Appl. Phys. **16**, 1891 (1977).
[11] M. Hikosaka, S. Minomura, and T. Seto, Jpn. J. Appl. Phys. **19**, 1763 (1980).
[12] M. Hikosaka, K. Tsukijima, S. Rastogi, and A. Keller, Polymer **33**, 2502 (1992).
[13] T. Seto, T. Hara, and K. Tanaka, Jpn. J. Appl. Phys. **7**, 31 (1968).
[14] K. E. Russell, B. K. Hunter, and R. D. Heyding, Polymer **38**, 1409 (1997).
[15] H. Miyaji, T. Asahi, Y. Miyamoto, and K. Asai, J. Polym. Sci., Part B: Polym. Phys. **25**, 159 (1987).
[16] D. J. Pastine, J. Chem. Phys. **49**, 3012 (1968).
[17] M. Kobayashi, J. Chem. Phys. **70**, 509 (1979).
[18] M. S. Miao, M. L. Zhang, V. E. Van Doren, C. Van Alsenoy, and J. L. Martins, J. Chem. Phys. **115**, 11317 (2001).
[19] J. Leger, C. Chateau, and A. Lacam, J. Appl. Phys. **68**, 2351 (1990).
[20] F. Datchi, R. LeToullec, and P. Loubeyre, J. Appl. Phys. **81**, 3333 (1997).
[21] A. P. Hammersley, S. O. Svensson, M. Hanfland, A. N. Fitch, and D. Häusermann, High Press. Res. **14**, 235 (1996).
[22] http://www.quantum-espresso.org; S. Scandolo, P. Giannozzi, C. Cavazzoni, S. de Gironcoli, A. Pasquarello, and S. Baroni, Z. Kristallogr. **220**, 574 (2005).
[23] J. P. Perdew, K. Burke, and M. Ernzerhof, Phys. Rev. Lett. **77**, 3865 (1996).
[24] D. Vanderbilt, Phys. Rev. B **41**, 7892 (1990).
[25] P. A. Doyle and P. S. Turner, Acta Crystallogr., Sect. A: Cryst. Phys., Diffr., Theor. Gen. Crystallogr. **24**, 390 (1968).
[26] http://www.isis.rl.ac.uk/ISISPublic/reference/Xray_scatfac.htm
[27] D. L. Dorset, Macromolecules **66**, 1175 (1991).
[28] P. Vinet, J. Ferrante, J. R. Smith, and J. H. Ross, J. Phys. C **19**, L467 (1986).